Robust Vibration Control of a Plate Using Self-sensing Actuators of Piezoelectric Patches

WENFENG ZHANG,* JINHAO QIU AND JUNJI TANI

Institute of Fluid Science, Tohoku University, Katahira 2-1-1, Aoba-Ku, Sendai, 980-8577, Japan

ABSTRACT: Piezoelectric actuators and sensors are increasingly being used in applications involving vibration/position/shape control devices. Based on the self-sensing actuator (SSA) concept in which the sensors and actuators are seamlessly collocated, this paper presents a study on the robust control of a clamped plate. An analytical model of a plate with surface-bonded piezoelectric patches is derived and a μ-synthesis controller is designed to suppress multi-mode vibrations of the clamped plate under perturbations. The experimental results show that the symmetrical and asymmetrical modes can be effectively suppressed with designed feedback control using two piezoelectric patches which are positioned symmetrically and asymmetrically on the plate, respectively.

Key Words: self-sensing actuator, clamped plate, μ-synthesis, parameter uncertainty, unmodeled dynamics

INTRODUCTION

PIEZOELECTRIC materials have been widely used as sensors and actuators owing to their excellent transducing properties between the electrical and mechanical strain energies, and independent piezoelectric devices for the sensors and actuators are generally necessary. With the self-sensing actuator (SSA in short) techniques proposed by Dosch and Inman (1992) however, it is now possible to make a single piece of piezoelectric material assume the roles of the traditional sensor and actuator concurrently. One of the merits of the SSA is the true collocation of the sensor and the actuator, which may lead to better closed-loop stability. The other is the elimination of the possible capacitive coupling between the sensor and the actuator. As a result, the SSA has attracted considerable attention from many researchers over the past decade. For example, Anderson et al. (1992) converted the equation of a cantilevered beam into a state-space model and demonstrated experimentally the effectiveness of self-sensing piezoelectric actuators in suppressing vibrations. Dongi et al. (1996) implemented the concept of self-sensing piezoelectric actuators to the suppression of panel flutter. Ray et al. (1999) also applied SSA to the detection of structural damage. However, in these studies, the day-to-day changes in the piezoelectric capacitances proved significant enough to require a readjustment of the circuit bridge to extract an accurate measure of the mechanical strain rate. Vipperman and Clark (1996) invented a hybrid analog and digital adaptive compensator to extract mechanical strain. Based on Vipperman's work, Fannin (1997) designed an analogous adaptive piezoelectric sensoriactuator. Jiang et al. (1996) extended their analysis to nonlinear hysteretic behaviors. On the one hand, most of the current studies apply SSA only to simple beam-like structure for detecting structural damage, for suppressing the structural vibration, and so on. On the other hand, the current results showed the effectiveness only in the SISO experimental tests. For the MIMO cases, few results have been reported. Due to the coupling between multi-set of SSAs, the design of MIMO controllers is significantly more complex and demanding than the SISO case in terms of control performance, stability, and robustness. Up to this point, there is no sufficient experimental evidence using the MIMO scheme for vibration suppression using the SSA techniques.

In the control design phase, two facts should be taken into consideration. One is that the capacitance of piezoelectric patches is sensitive to temperature, light, and the laden voltage. Hence, it is necessary to include the capacitance uncertainty in the circuit model. The other is that usually, due to the complex nature of the physical system, a low-order and nominal model that describes the low–mid frequency range behavior of the plant is available, but the high-frequency behavior is unknown, and even the dynamic order of the actual system is unknown. This means that the control should be robust against variations due to unmodeled dynamics and structural uncertainty. Moreover, the mathematical model between the disturbance force and the structure is

*Author to whom correspondence should be addressed.
E-mail: zhang@mozart.ifs.tohoku.ac.jp

1045-389X/04/12 0923–9 $10.00/0 DOI: 10.1177/1045389X04045153

difficult to obtain. To the best of the authors' knowledge, however, the current studies paid little attention to the problem of robustness. Law et al. (2003) proposed an adaptive compensation combined with the SSA technique to simultaneously suppress beam vibrations during piezoelectric capacitance variance. Halim and Moheimani (2002) developed a spatial H-infinity control for the vibration control of a beam-like structure. Hence, how to design a μ-controller is of great interest in the application of SSA technique.

In this paper, a smart board under noise whose response is suppressed by two self-sensing actuators is considered. It emphasizes the robustness of the control against parametric as well as structural uncertainty. In "Electromechanical Coupling Characteristics of the Clamped Plate System," an analytical model in mode space is derived using the structural analysis software ANSYS, in which the electromechanical coupling dynamics among a plate, piezoelectric patches, and compensator bridges that read out the mechanical dynamics are taken into consideration. The board model includes lots of modes and is simplified to the first five modes that are not involved in an internal resonance with other modes since the first five natural frequencies given by the modal analysis are in very good agreement with the experimental data. Then in "Robust Controller Design," by using μ-analysis and synthesis shown in Oshima et al. (1997) a μ-controller is designed to consider three primary concerns which are as follows: (1) the presence of disturbances in both the input and output of the system; (2) the lack of full state information of the coupling electromechanical system, just the sensor signals from the compensator bridges; and (3) robust control that is insensitive to noise, model uncertainty, and piezoelectric capacitance change. Finally, experimental results are given to validate these studies.

ELECTROMECHANICAL COUPLING CHARACTERISTICS OF THE CLAMPED PLATE SYSTEM

Piezoelectric Sensor and Actuator Equations

The equivalent model of a piezoelectric element proposed by Dosch and Inman (1992) was extended to the two-dimensional case shown in the following equation

$$v_p(t) = -\frac{Y_p r_1}{(1-\mu_p^2)C_p^s}\int_{A_p}\left[\frac{\partial^2 w(x,y,t)}{\partial x^2}(d_{31}+d_{32}\mu_p) + \frac{\partial^2 w(x,y,t)}{\partial y^2}(\mu_p d_{31}+d_{32})\right]dA_p, \tag{1}$$

where v_p is the voltage across the piezoelectric produced by the mechanical strain. The system parameters are described in Tables 1 and 2.

Table 1. Parameters of the G(s) system.

Young's modulus, Y	6.9×10^{10} N/m^2
Density, ρ	2699 kg/m^3
Poisson's ratio, μ	0.345
Length, a/b	0.13 m
Thickness, h	0.001 m
Capacitance, C_1	120 nF
Resistor, R_p	2000 Ω
Variable resistor, R_1	688 Ω (0–2000 Ω)

Table 2. Parameters of the piezoelectric patches.

Young's modulus, Y_{11}	5.9×10^{10} N/m^2
Young's modulus, Y_{33}	5.2×10^{10} N/m^2
Young's modulus, Y_{55}	2.1×10^{10} N/m^2
Charge constant, d_{31}	-260×10^{-12} m/V
Charge constant, d_{33}	540×10^{-12} m/V
Charge constant, d_{15}	750×10^{-12} m/V
Capacitance, C_p^s	123 nF
Density, ρ_p	7400 kg/m^3
Permittivity, $\varepsilon_{11}/\varepsilon_0$	3100 ± 250
Permittivity, $\varepsilon_{33}/\varepsilon_0$	3400 ± 270
Poisson's ratio, μ_p	0.34
Length, a_p/b_p	0.03 m
Thickness, h_p	0.0002 m
Loss tangent	1.8
$r_1 = h + h_p/2$	0.0006 m

A method developed by Griffin and Henderson (1997) which treats the actuation of the PZT as the blocked force acting on the plate and PZT patch, was used. This force results in a distributed moment around the edge of the wafer, as shown in Figure 1. These distributed moments are

$$\begin{aligned} M_x &= d_{31}Y_p\frac{h+h_p}{2}V_a\chi_{A_p} = K_{ax}V_a\chi_{A_p},\\ M_y &= d_{32}Y_p\frac{h+h_p}{2}V_a\chi_{A_p} = K_{ay}V_a\chi_{A_p} \end{aligned} \tag{2}$$

where M_x and M_y are the bending moments generated by the piezoelectric actuator in the x- and y-directions respectively. V_a is the applied voltage and χ_{A_p} can be obtained from the equation as given below

$$\chi_{A_p} = [H(x-x_1)-H(x-x_2)]\times[H(y-y_1)-H(y-y_2)], \tag{3}$$

where x_1, x_2, y_1, and y_2 are the PZT coordinates configured in Figure 1 respectively and $H(x)$ is the Heaviside step function.

Compensator Circuit Model

In a practical implementation of the self-sensing actuator, the model of the piezoelectric patch is shown in Figure 2(a) and the bridge shown in Figure 2(b) is used to sense the rate of strain. In this circuit bridge, V_c (in the frequency domain) is an external control voltage

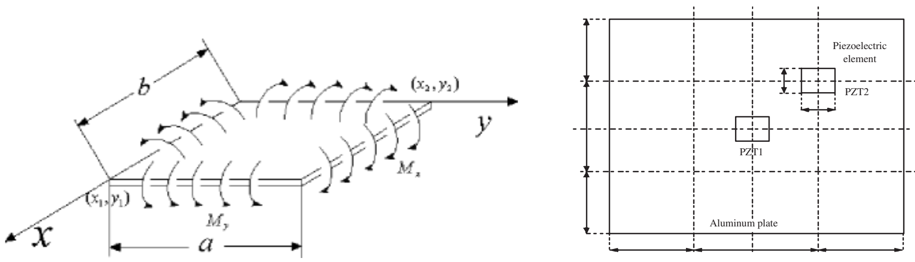

Figure 1. *(a) Distributed moment and (b) the positions of PZTs.*

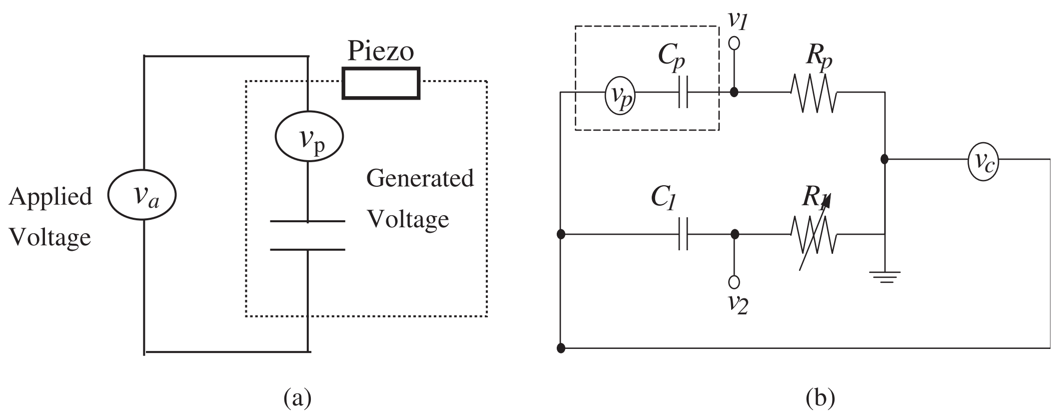

Figure 2. *(a) The model of the PZT and (b) the rate of strain sensing circuit.*

applied to the structure. The ideal output of the bridge circuit V_s (in the frequency domain) is defined as:

$$V_s = V_2 - V_1 = \frac{R_p C_p s}{R_p C_p s + 1} V_p, \tag{4}$$

where

$$R_p C_p = R_1 C_1. \tag{5}$$

Electromechanical Coupling Structure Model

In this paper, we consider a structure composed of a plate and two pieces of piezoelectric elements as shown in Figure 3. The equation of motion of this smart plate structure with externally applied control moments becomes:

$$\begin{aligned}
&\ddot{\xi}_q + 2\varsigma_q \omega_q + \omega_q^2 \xi_q = P_q(t) \\
&P_q(t) = \iint_{A_p} p(x,y,t) W_q dxdy \\
&\qquad + K_{ax} V_a \int_{y_1}^{y_2} [W'_{qx}(x_1,y) - W'_{qx}(x_2,y)]dy \\
&\qquad + K_{ay} V_a \int_{x_1}^{x_2} [W'_{qy}(x,y_1) - W'_{qy}(x,y_2)]dx \\
&\quad = \iint_{A_p} p(x,y,t) W_q dxdy + K_{ax} V_a \theta_q
\end{aligned} \tag{6}$$

where $p(x,y,t)$ is the distributed external force within the area of the plate (in the direction of the z-axis), q represents the modal numbers, ω_{pq} is the natural frequency, ς is the mode damping, V_a is the applied voltage shown in Figure 2(a), $W_q(x,y)$ is the modal shape, and W'_{qx} and W'_{qy} stand for $\partial W_q/\partial x$ and $\partial W_q/\partial y$, respectively.

Hence, the state space equation can be expressed in the following form:

$$\begin{aligned}
&\begin{bmatrix} \dot{\xi} \\ \ddot{\xi} \end{bmatrix} = A \begin{bmatrix} \xi \\ \dot{\xi} \end{bmatrix} + BV_a;\ V_p = C \begin{bmatrix} \xi \\ \dot{\xi} \end{bmatrix} \\
&C = -\frac{K_{ax}}{(1-\mu_p)C_p} [\theta_1 \cdots \theta_q\ 0 \cdots 0] \\
&A = \begin{bmatrix} 0 & \cdots & 0 & 1 & \cdots & 0 \\ \vdots & \ddots & \vdots & \vdots & \ddots & \vdots \\ 0 & \cdots & 0 & 0 & \cdots & 1 \\ -\omega_1^2 & \cdots & 0 & -2\varsigma_1\omega_1 & \cdots & 0 \\ \vdots & \ddots & \vdots & \vdots & \ddots & \vdots \\ 0 & \cdots & -\omega_q^2 & 0 & \cdots & -2\varsigma_q\omega_q \end{bmatrix} \\
&B = \begin{bmatrix} 0 \\ \vdots \\ 0 \\ K_{ax}\theta_1 \\ \vdots \\ K_{ax}\theta_q \end{bmatrix}.
\end{aligned} \tag{7}$$

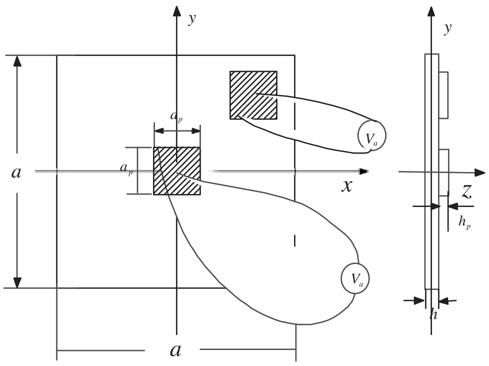

Figure 3. Schematic diagram of the smart plate structure.

ROBUST CONTROLLER DESIGN

In general, the design of robust control includes the synthesis of the controller and the selection of weighting functions. The consideration of the physical system is crucial. The so-called physical system includes the capacitance uncertainty and unmodeled dynamics.

Parametric Uncertainty in Compensator Circuit

The capacitance of piezoelectric patches is sensitive to temperature, light, and the laden voltage. As expressed in Equation (5), the varied capacitance will affect the RC bridge performance. Hence, it is necessary to include the capacitance uncertainty in the circuit model. The capacitance varies in the range

$$\begin{aligned} &C_{p\min} \leq C_p \leq C_{p\max} \\ &W_k = \max\left(\frac{(C_{p\max} - C_p)}{C_p}, \frac{(C_p - C_{p\min})}{C_p}\right); \\ &C_p = \bar{C}_p(1 + W_k\delta_c), \quad -1 \leq \delta_c \leq 1 \end{aligned} \tag{8}$$

where $C_{p\max}$, $C_{p\min}$ are the maximum and the minimum capacitance and $\bar{C}_p$ is the average one.

According to Balas et al. (1995) the uncertain characteristic in the compensator circuit can be formulated as follows:

$$\begin{aligned} \begin{bmatrix} \dot{v}_1 \\ \dot{v}_2 \end{bmatrix} = &\left(\begin{bmatrix} -\dfrac{1}{C_pR_p} & 0 \\ 0 & -\dfrac{1}{C_1R_1} \end{bmatrix} + \delta_c \begin{bmatrix} \dfrac{W_k}{R_p} & 0 \\ 0 & 0 \end{bmatrix}\right) \begin{bmatrix} v_1 \\ v_2 \end{bmatrix} \\ &+ \left(\begin{bmatrix} 1 & 1 \\ 0 & 1 \end{bmatrix} + \delta_c \begin{bmatrix} -W_k & 0 \\ 0 & 0 \end{bmatrix}\right) \begin{bmatrix} \dot{v}_p \\ \dot{v}_c \end{bmatrix}. \end{aligned} \tag{9}$$

where v_1, v_2 are the sensor voltages shown in Figure 2(b), and v_c is the control voltage (in the time domain).

Plant Perturbation

Owing to the complex nature of physical systems, usually, a low-order and nominal model, which describes the low–mid frequency range behavior of the plant, is available, but the high-frequency behavior is unknown. In this situation, even the dynamic order of the actual system is unknown, and something richer than parametric uncertainty is needed to represent this uncertainty. Roughly, this allows one to specify a frequency-dependent percentage uncertainty in the actual system behavior. In order to specify the uncertainty plant set, the following need to be chosen:

- A nominal model, $G(s)$, and
- A multiplicative uncertainty weighting function, $W_{vc}(s)$.

Given these functions, the precise definition of the multiplicative uncertainty plant set is

$$\mathrm{M}(G, W_{vc}) := \left\{\tilde{G}: \left|\frac{\tilde{G}(j\omega) - G(j\omega)}{G(j\omega)}\right| \leq \left|W_{vc}(j\omega)\right|\right\} \tag{10}$$

Control Scheme and the Selection of Weighting Functions

Utilizing the structured singular value μ, we design the controller, which achieves the robust performance against various types of uncertainties. Interconnection structure by LFT is represented in Figure 4. In the diagram, $G(s)$ denotes the nominal dynamics and $K(s)$ denotes the feedback controller. The perturbation $\Delta(s)$ defines the model variations. However, they are not known explicitly. All that is known of the perturbation is that its infinity norm is bounded to be strictly less than unity, i.e. $\|\Delta(s)\| < 1$. The multiplicative uncertainty W_{vc} is used to scale the effects of $\Delta(s)$ and define the bounds up to which the model varies. The parameter uncertainty δ_c defines the physical parameter variations as illustrated in "Parametric Uncertainty in Compensator Circuit." W_y is the unknown disturbance and will be discussed in the next section, W_{vs} represents the sensor noise, W_e is the normalized performance specification, W_{filt} is a band filter, and W_g is the post-compensator for improving the performance at the low-frequency range. The output e is the weighted voltage by a performance weighting function W_e.

We define the block structure Δ as follows.

$$\mathbf{\Delta} = \left\{\mathrm{diag}[\delta_{\mathbf{c}}, \Delta(s)]: \delta_c \in \mathbf{R}^{m\times m}, \Delta(s) \in \mathbf{C}^{n\times n}\right\} \tag{11}$$

It is well known that the structured singular value $\mu_\Delta(M)$ is defined for matrices $M \in \mathbf{C}^{n\times n}$ with the block

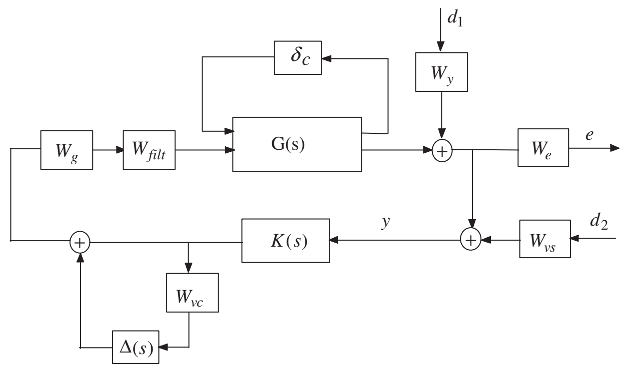

Figure 4. *Generalized and weighted performance block diagram.*

structure $\mathbf{\Delta}$ as

$$\mu_\Delta(M) = \frac{1}{\min\{\bar{\sigma}(\Delta)\colon \Delta \in \mathbf{\Delta}, \det(I - M\Delta) = 0\}} \tag{12}$$

Unless no $\Delta \in \mathbf{\Delta}$ makes $I - M\Delta$ singular, in which case $\mu_\Delta(M) = 0$. Then the objective of μ-synthesis is to design a controller $K(s)$ satisfying the following constraint condition, where $\hat{G}(s)$ is the generalized plant which is interconnected with weighting function.

$$\sup_{\omega \in R} \mu_\Delta[F_l(\hat{G}(j\omega), K(j\omega)] < 1 \tag{13}$$

We apply the standard D–K iteration to find the suboptimal μ-controller for the system. We thus iteratively solve the following problem:

$$\sup_{\omega \in R} \inf_{D(\omega)} \left\{ \bar{\sigma}(D(j\omega) F_l(\hat{G}, K) D^{-1}(j\omega) \right\} < 1 \tag{14}$$

As is known, the weightings are included in controller synthesis instead of in control system implementation to yield robust performance and stability. In general, in order to find a controller, they should be properly selected in advance.

Choice of W_{vs}: The weight W_{vs} represents the frequency domain models of the sensor noise. The sensor measurement feedback to the controller has some noise, which is higher in the high-frequency band than in the low-frequency band, as shown below:

$$W_{vs} = \frac{0.005s + 5}{0.0001s + 1}. \tag{15}$$

Choice of W_{vc}: The weighting function W_{vc} is selected with respect to the uncertainty boundary (proportional plant perturbation) as:

$$W_{vc} = \frac{0.0005s + 0.5}{0.0001s + 1}. \tag{16}$$

Choice of W_g: This post-compensator improves the performance at low frequencies. Therefore, W_g is selected by adding an integral function in order to achieve a low-frequency disturbance rejection. A phase-advance term is added to make the response faster. W_g has the following form:

$$W_g = \frac{s + 1000}{s + 8.327 \times 10^{-13}}. \tag{17}$$

Choice of W_{filt}, and W_e: The weighting function W_{filt}, i.e., a band pass filter, has been designed using MATLAB Toolbox to remove the direct current offset, the high frequency characteristics and noise generated by the post-compensator W_g. The normalized performance W_e has the same form as W_{filt}.

EXPERIMENTAL VERIFICATION

In this section, the results of the experimental evaluation of the feedback controller for the clamped plate with self-sensing actuators are presented.

Experimental Setup

The plate test setup of Figure 5 is made of AISI 2024 aluminum alloy with the dimensions 130 mm × 130 mm wide and 1mm thick. The plate is clamped on all sides by a 20 kg aluminum frame. Two rectangular piezoelectric patches ($30 \times 30\,\text{mm}^2$ wide and 0.2 mm thick) are bonded to the upper surface of the plate using an Araldite layer to isolate the electrode from the plate that is electrically grounded. The location of the piezoelectric transducers has been chosen to maximize its interaction with the first five bending modes of the plate derived from the ANSYS analysis. Each transducer is connected to a couple of dedicated electric terminals to be driven individually. These terminals are left electrically floating to ensure the inclusion of each transducer in the self-sensing bridge circuits. The plate is excited using an electromechanical speaker (FW227) driven by a power amplifier 2706, and the resulting response is measured with a laser displacement meter (LC-2400) to verify the control results. The analog signals from the compensator circuits were respectively amplified to differential amplifiers (Gains are 30 and 50 respectively), then sampled through an A/D converter and then transmitted to a DSP RTI1103. The designed controller is

Figure 5. *Configuration of the experimental setup.*

implemented digitally in DSP. The control input, calculated on the basis of the sensor signals, is amplified and then applied to the actuators. The gain of the power amplifier is 10. The overall setup is configured as shown in Figure 5.

Experimental Results

Information on the environmental disturbance W_y is roughly estimated. A speaker with a random noise signal excited the untreated plate and the sensor voltage is shown in the FFT analyzer. The estimated W_y both in magnitude and phase compared with experimental results is shown in Figure 6. The model developed in "Electromechanical Coupling Characteristics of the Clamped Plate System" is coincident with practical systems in the low-frequency range.

In a practical system, the experimental results on the performance of the compensator circuit bridge in extracting mechanical dynamics are less effective than the numerical results. Figure 7(a) shows both the compensated and uncompensated sensoriactuator plots. The uncompensated response is dominated by the feed through electrical dynamics. The modal resonances of the plate are barely detectable in these predominately first-order curves, corresponding to the magnitude and phase response. The self-sensing actuator responses appear along with the uncompensated response, some 20 dB below in magnitude. In addition, the PZT2 sensor signal of Figure 7(b) shows the detectable first mode characteristics when the voltage is applied to the self-sensing PZT1 actuator.

With the constructed model, the well-balanced bridge and, the previous choice of weighting functions, the controller is designed using the D–K iteration approach to μ-synthesis. Three D–K iterations yield a μ-controller of the 86th order. This controller is reduced to a 30th order μ-controller to facilitate practical applications by means of the optimal Hanker norm approximation. Furthermore, this controller is discretized with a zero-order hold for digital control. The sampling frequency is selected at 10 kHz. The speaker excites the plate and the displacements are measured at the centrical position of PZT2 by displacement laser. The control input voltages, calculated based on the sensor voltages, are shown in Figure 8. Figure 9 shows that the control results in vibration energy reductions in the time domain of about 50%. Figure 10 presents the resulting frequency responses under band limited noise excitation with and without controls at temperature 12°C. It is obvious from the results that when both PZT1 and PZT2 are connected, a damping effect can be obtained over a broad band. Note the approximately 15 dB attenuation obtained for the first mode. Also, a reduction of more than 10 dB at 449 Hz and 5 dB attenuation both in the third and fourth modes are obtained.

To investigate how much the vibration increases or decreases at a certain mode by disconnecting each PZT patch, the resulting responses are compared with that of the case in which both the self-sensing actuators are connected. Figure 11 shows the effect of disconnecting PZT2 with the circuit bridge. Because of the symmetric location of PZT1 and the symmetric structure, it is easy to understand that this case effectively suppressed the symmetric mode, i.e. the first and fifth modes. Figure 12 shows the effect of disconnecting PZT1 with the bridge circuit. PZT2 is useful for suppressing the unsymmetrical mode, i.e., from the second mode to the fourth mode. However, another unexpected phenomenon is that PZT2 can excite the plate vibration at 98 Hz, which may has arisen from the simple compensator circuit.

To investigate how much the vibrations increase or decrease with changing experimental temperature and exciting unmodeled dynamics, these resulting responses are compared with the case of Figure 10. Figure 13 shows the effect of the experimental temperature. In the temperature range from 0 to 26°C, the control performance is still good and only the second model is a little deteriorated by about 3 dB at 0°C. Figure 14 shows

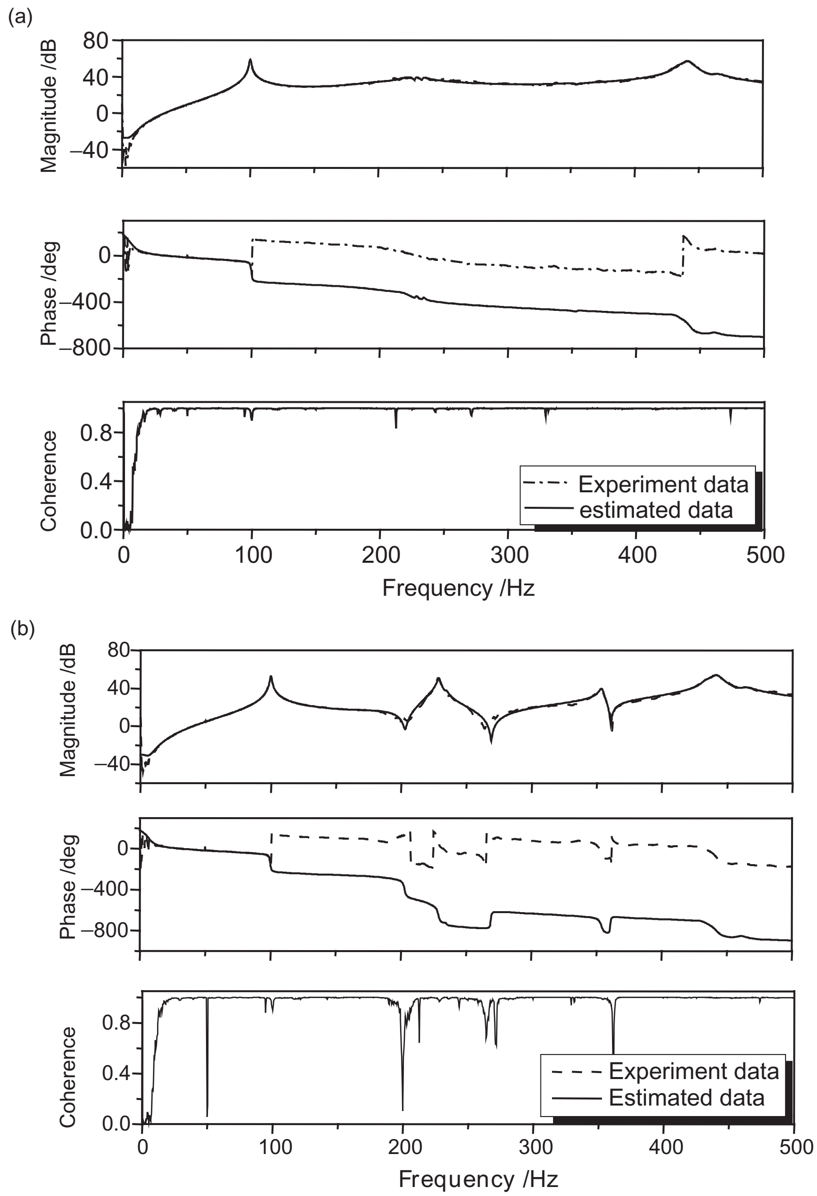

Figure 6. *(a) Estimated $W_y(1)$, which is from the disturbance speaker to PZT1 and (b) estimated $W_y(2)$, which is from the disturbance speaker to PZT2.*

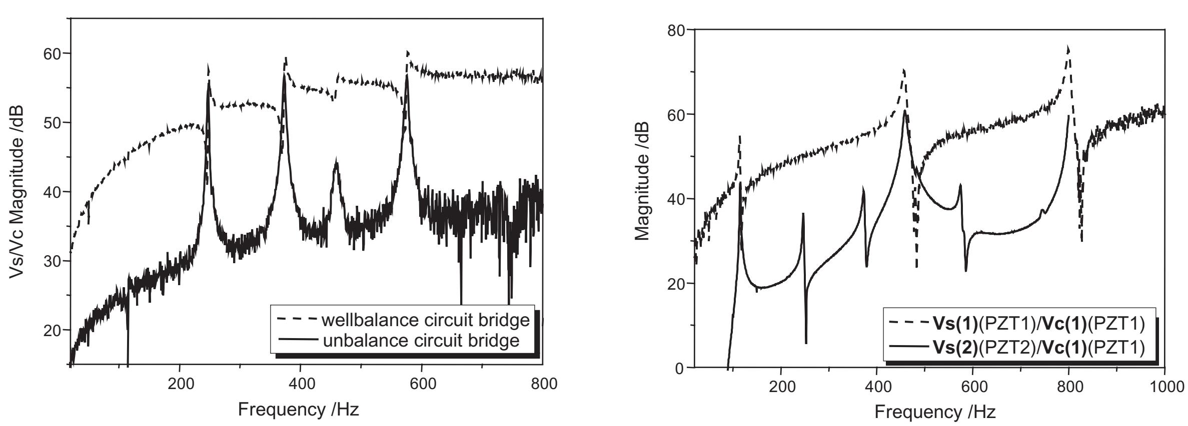

(a) Vs(2)(PZT2) Versus Vc(2)(PZT2)

(b) Vs Versus Vc(1)(PZT1)

Figure 7. *Frequency response of the sensor signal from the PZT vs the control voltage input to the PZT.*

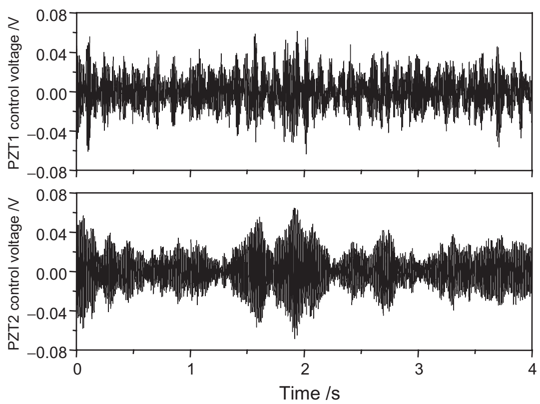

Figure 8. Control voltages.

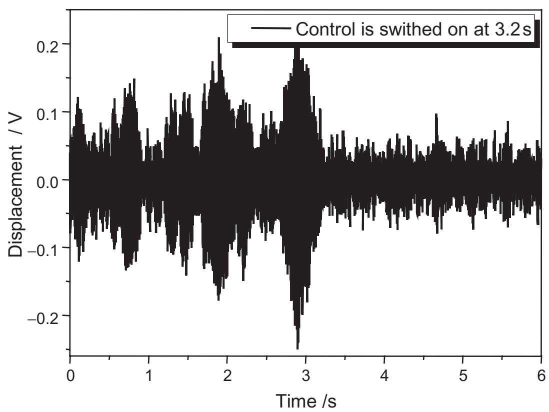

Figure 9. Time history of the displacement at PZT2.

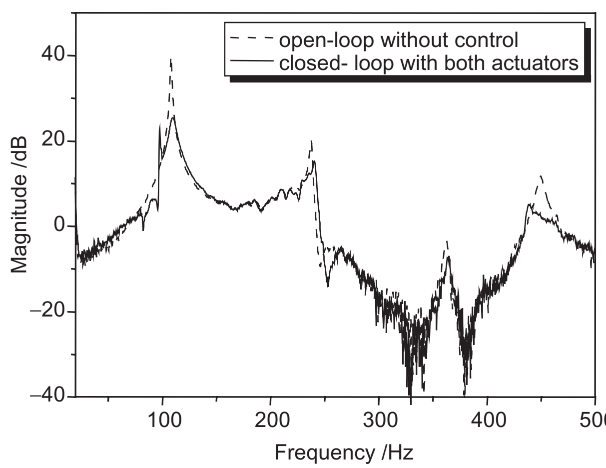

Figure 10. The resulting frequency response at the centrical position of PZT2 with and without control.

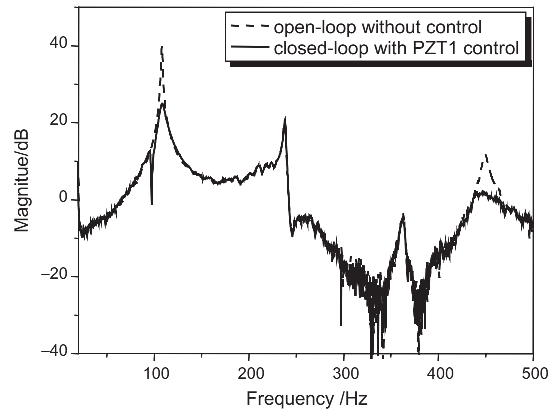

Figure 11. The resulting frequency response at the centrical position of PZT1 when the PZT1 actuator is turned on compared with when PZT1 and PZT2 are switched off.

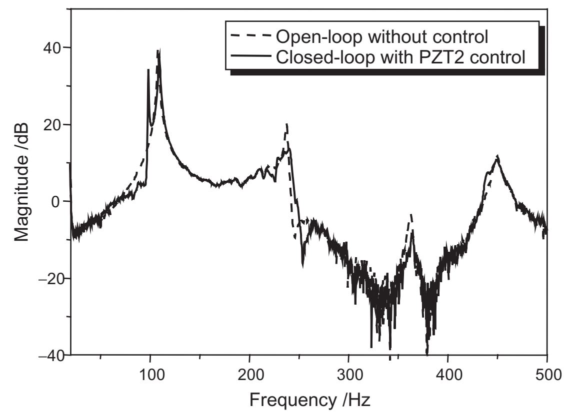

Figure 12. The resulting frequency response at the centrical position of PZT2 when the PZT2 actuator is turned on compared with when PZT1 and PZT2 are switched off.

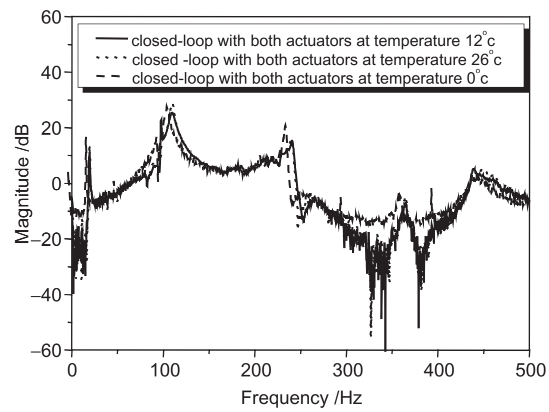

Figure 13. Control performance robustness against temperature fluctuations.

the effect of unmodeled dynamics. It can be seen that the unmodeled dynamics only slightly affect the control performance because of the robustness of the μ-synthesis controller.

CONCLUSIONS

In this paper, the fundamental issues regarding the vibration characteristics of plates with self-sensing

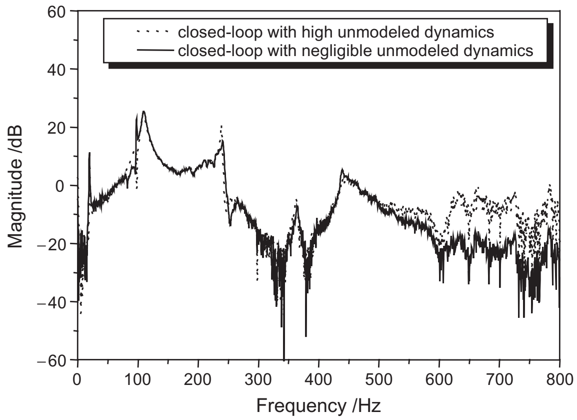

Figure 14. *Control performance robustness against unmodeled dynamics.*

piezoelectric patches were investigated. The obtained experimental results validated the electromechanical model developed in "Electromechanical Coupling Characteristics of the Clamped Plate System." Furthermore, robust μ-synthesis control theory is successfully applied to multi-set of SSAs, which have never been successful in a practical MIMO structure application. The experimental results show that the self-sensing actuator driven by the designed controller exhibits good performance in suppressing the multi-mode vibrations of the clamped plate in the low-frequency range. Also, the closed-loop stability over the whole range of plant perturbation was guaranteed by μ-synthesis control design. In addition, the SSA system with a μ-synthesis controller demonstrated robustness against noise, temperature, and so on. These results are very promising in providing broadband attenuation of plate vibration using self-sensing actuators.

With increasingly strict requirements for control speed and system performance, the unavoidable time delays in all digital controllers, analogue anti-aliasing and reconstruction filters, and the hysteretic characteristic of piezoelectric patch have become a serious problem. A further discussion on stability will be the subject of future work.

ACKNOWLEDGMENT

The authors would like to thank Dr. Zhu, Y. and all the people of the Intelligent Systems Laboratory in Tohoku University for their efforts and cooperation.

REFERENCES

Anderson, E.H., Hagood, N.W. and Goodliffe, J.M. 1992. Self-sensing Piezoelectric Actuation: Analysis and Application to Controlled Structures, In: *Proceedings of the AIAA/ASME/ASCE/AHS/ASC 33rd Structures, Structural Dynamics, and Materials Conference (Dallas, TX), AIAA*, Washington, DC, pp. 2141–2155.

Balas, G.J., Doyle, J.C., Glover, K., Packard, A. and Smith, R. 1995. *μ-Analysis and Synthesis Toolbox User's Guide*, The Math Works, Inc., Natick, MA, USA

Dongi, F., Dinkler, D. and Kroplin, B. 1996. Active Panel Flutter Suppression Using Self-sensing Piezoactuators, *AIAA Journal*, 34(6):1224–1230.

Dosch, J.J., Inman, D.J. and Garcia, A. 1992. A Self-sensing Piezoelectric Actuator for Collocated Control, *Journal of Intelligent Material Systems and Structures*, 3(1):166–185.

Fannin, C.A. 1997. Design of Analogy Adaptive Piezoelectric Sensoriactuator. Master Thesis, Virginia Polytechnic Institute and State University.

Griffin, S. and Henderson, B. (April 1997). An Investigation into Inaccuracies in Closed-form Piezoceramic Actuator Models for Smart Structures, In: *Proceedings, AIAA Structures, Structural Dynamics and Materials Conference*, (Kissimmee, FL), AIAA paper 97–1309.

Halim, D. and Moheimani, S. 2002. Experimental Implementation of Spatial H-Infinity Control on a Piezoelectric Laminate Beam, *IEEE-ASME Transactions on Mechatronics*, 7(3):346–356.

Jiang, Z., Chonan, S. and Yamamoto, T. 1996. Self-sensing Feedback Compensation of Non-linear Hysteretic Piezoceramic Actuators, In: *Seventh International Conference on Adaptive Structures*, Sept. 23–25, Rome, Italy.

Law, W.W., Liao, W.-H. and Huang, J. 2003. Vibration Control of Structures with Self-sensing Piezoelectric Actuators Incorporating Adaptive Mechanisms, *Smart Materials and Structures*, 12(5): 720–730.

Oshima, K., Takigami, T. and Hayakawa, Y. 1997. Robust Vibration Control of a Cantilever Beam Using Self-sensing Actuator, *JSME International Journal Series C-Mechanical Systems Machine Elements and Manufacturing*, 40(4):681–687.

Ray, L.R. and Tian, L. 1999. Damage Detection in Smart Structures Through Sensitivity Enhancing Feedback Control, *Journal of Sound and Vibration*, 227(5):987–1002.

Vipperman, J.S. and Clark, R.L. 1996. Implementation of an Adaptive Piezoelectric Sensoriactuator, *AIAA Journal*, 34(10):2102–2109.